Research Square

Preprints are preliminary reports that have not undergone peer review.
They should not be considered conclusive, used to inform clinical practice,
or referenced by the media as validated information.

A New Global Vulnerability Model for Regional Seismic Risk Assessments: Part 1 – Structural Vulnerability

Karim Aljawhari

k.aljawhari@ucl.ac.uk

GEM Foundation https://orcid.org/0000-0003-4891-8702

Al Mouayed Bellah Nafeh

GEM Foundation

Vitor Silva

GEM Foundation

Research Article

Keywords: vulnerability, fragility, structural performance, earthquake, losses, multi-degree-of-freedom, regional

Posted Date: November 7th, 2025

DOI: https://doi.org/10.21203/rs.3.rs-7935593/v1

License: This work is licensed under a Creative Commons Attribution 4.0 International License.
Read Full License

Version of Record: A version of this preprint was published at Bulletin of Earthquake Engineering on June 5th, 2026. See the published version at https://doi.org/10.1007/s10518-026-02443-7.

A New Global Vulnerability Model for Regional Seismic Risk Assessments: Part 1 – Structural Vulnerability

Karim Aljawhari[1,2*], Al Mouayed Bellah Nafeh[1], Vitor Silva[1,3]

[1]*Global Earthquake Model (GEM) Foundation, Pavia, Italy*

[2]*Department of Civil, Environmental, and Geomatic Engineering, University College London (UCL), London, UK*

[3]*Department of Civil Engineering, University of Aveiro, Aveiro, Portugal*

*Corresponding Author. Email Address: k.aljawhari@ucl.ac.uk

ABSTRACT

Reliable vulnerability functions are essential for earthquake risk assessment, yet those currently used in regional and large-scale contexts often rely on numerical models that oversimplify the complex behaviour of buildings. This can lead to biased predictions of structural performance and earthquake-induced losses. In the new Global Vulnerability Model supported by the Global Earthquake Model (GEM) Foundation, we present an improved structural vulnerability database for seismic risk assessment, featuring four key advances: 1) the number of building classes has been expanded from approximately 500 classes to over 1,400 to consider additional structural systems and seismic code levels; 2) an improved numerical modelling strategy that simulates the seismic response using efficient multi-degree-of-freedom *stick-and-mass* models; 3) an extensive dataset of ground motion records for response analysis covering diverse tectonic settings (e.g., active shallow crust, stable continental, and subduction zones), and 4) a new suite of vulnerability functions addressing specifically structural damage. This contribution describes the vulnerability modelling for structural components, which is used to compute damage and monetary losses within the scope of GEM's Global Seismic Risk Model. The derived vulnerability functions in this study are available in an open-access repository for use in both probabilistic and scenario-based seismic risk assessments.

Keywords: vulnerability; fragility; structural performance; earthquake, losses; multi-degree-of-freedom; regional

1. INTRODUCTION

Earthquakes pose an important threat to life and property, with more than one million deaths and nearly a trillion USD in economic losses recorded over the past century (Sen 2009; Elnashai and Di Sarno 2015). These catastrophic figures are largely due to the poor performance of structures that fail to meet seismic design standards (e.g., Bull 2013; So 2016; Gautam and Chaulagain 2016). Reliable structural vulnerability models are therefore essential for seismic risk analyses, shaping both our understanding of risk drivers and strategies for disaster mitigation and resilience planning. While a holistic vulnerability framework must ultimately account for losses related to structural/non-structural components and building contents, the structural performance remains the cornerstone of seismic risk models.

As part of the first Global Seismic Risk Model (Silva et al. 2020) developed by the Global Earthquake Model (GEM) Foundation in 2018, Martins and Silva (2021) introduced a database of fragility and vulnerability functions. Fragility functions describe the probability of exceeding a set of damage states (DSs), conditioned on a suitable ground-shaking intensity measure (IM). These functions were then combined with damage-to-loss ratios (e.g., Dolce et al. 2006; FEMA 2012), which link each DS to an expected loss, expressed as a fraction of the building's replacement cost. This process leads to vulnerability functions characterising the loss ratio across a range of IM levels (e.g., Martins et al. 2016; Aljawhari et al. 2024). The database of Martins and Silva (2021) covered about 500 building classes and simulated their seismic performance by generating simplified single-degree-of-freedom (SDOF) oscillators and assessing their performance through nonlinear time-history analyses (NLTHA).

Martins and Silva (2021) database marked an important step in making vulnerability functions available on a global scale, yet its reliance on SDOF oscillators and simplified modelling assumptions remains a major limitation. SDOF models are effective in evaluating the global behaviour of first-mode dominated structures, but they fall short in simulating more complex mechanisms like inelastic demand concentration and higher-mode effects (e.g., Nettis et al. 2021; Suzuki and Iervolino 2021; Angelucci et al. 2022).

They also cannot reproduce storey-level seismic demand parameters, like peak storey drifts (PSD) and peak floor acceleration (PFA), which are essential for damage and loss assessment in multi-storey buildings, especially for non-structural components and building contents. Other limitations include the relatively limited set of ground-motion records used for the NLTHA.

To overcome these challenges, building-specific risk assessment approaches, such as the FEMA P-58 (Günay and Mosalam 2013), have gained traction. These approaches compute losses at the component level and often utilise refined multi-degree-of-freedom (MDOF) models that simulate the inelastic mechanisms of individual building components. They also require hazard-consistent ground-motion records and extensive inventories of fragility and loss models for all building components. While these approaches are effective for detailed, single-building assessments, their computational demand makes them impractical for large-scale regional applications. To balance the accuracy of detailed MDOF models with the efficiency of SDOF oscillators, particularly for regional studies, several researchers have recommended using mechanical MDOF systems like *fish-bone* models (e.g., Soleimani et al. 2019; Jamšek and Dolšek 2020) or *stick-and-mass* models (e.g., Xiong et al. 2016; Lu et al. 2018; Gaetani d'Aragona et al. 2020). These representations can capture the shear response of individual storeys, allowing reliable estimates for interstorey seismic demands with significantly lower computational effort.

Despite the above advancements, a comprehensive database of reliable MDOF models encompassing a broad range of building classes, along with refined fragility and vulnerability functions, remains unavailable. To bridge this gap, our study leverages Martins and Silva (2021) database and introduces four major innovations: 1) expanding the covered building classes from approximately 500 to over 1,400; 2) advancing the numerical modelling strategy by replacing the original SDOF oscillators with *stick-and-mass* MDOF systems, enabling explicit analysis of storey demands and more complex inelastic mechanisms; 3) compiling a more comprehensive dataset of ground-motion records with diverse tectonic environments to be used in NLTHA; and 4) deriving a new suite of structural fragility and vulnerability functions that provide a more realistic prediction of seismic damage and loss for all building classes. The new database is compared against the original version, unveiling key differences that underscore the role of robust modelling for regional risk assessments.

This paper constitutes the first part of GEM's new Global Vulnerability Model, focusing on the numerical modelling strategy, analysis approach, and the derivation of structural fragility and vulnerability functions. A companion paper (Part II) extends this work by addressing seismic losses incurred by non-structural components and building contents. The complete suite of fragility and vulnerability functions is used for assessing damage and economic losses within the 2026 version of the Global Seismic Risk Model and are publicly available on GitHub[1].

2. NEW GLOBAL VULNERABILITY DATABASE: METHODOLOGY

The methodology adopted to develop the new global vulnerability database is outlined in Figure 1. The process begins with the numerical modelling of *stick-and-mass* MDOF systems for over 1,400 building classes. The nonlinear dynamic behaviour of the models is assessed via a cloud-based NLTHA (Cornell et al. 2002; Jalayer et al. 2017), adopting a new extensive suite of ground-motion records. These results are then used to derive fragility functions that characterise structural damage conditional on a ground-shaking IM. Finally, structural vulnerability functions are generated by combining the fragility functions with suitable damage-to-loss ratios, yielding a comprehensive set of functions for estimating structural losses for a large variety of building classes worldwide. We detail each step in the following sections.

[1] https://github.com/gem/global_vulnerability_model/tree/v2025.0.0

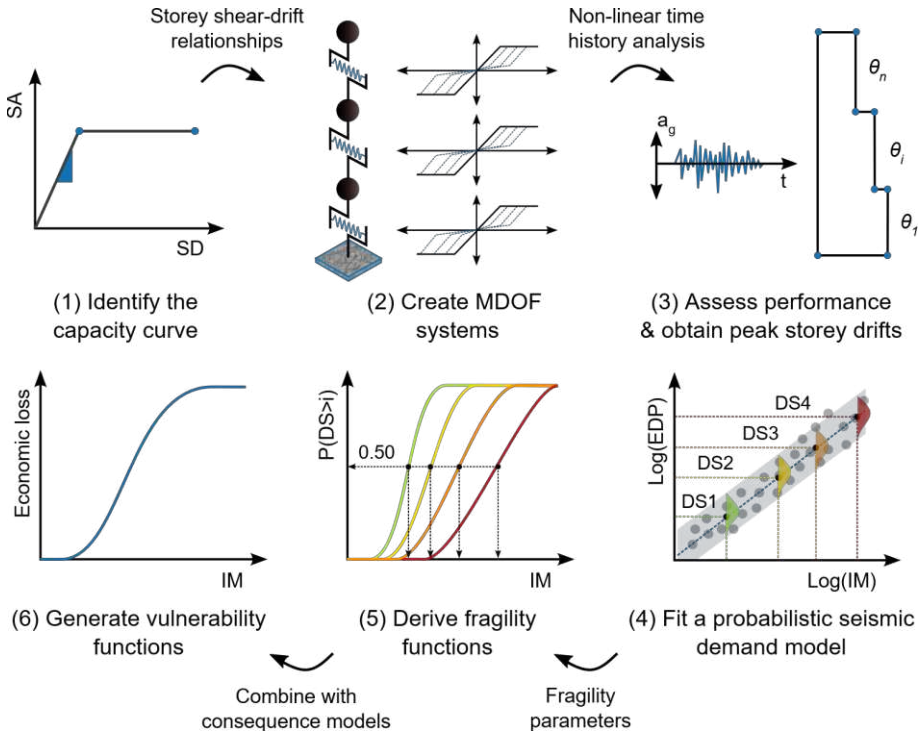

Figure 1. Methodology of the derivation of structural fragility and vulnerability functions.

2.1. Definition of Building Classes and Capacity Curves

The new vulnerability database expands the building classes to over 1,400, encompassing a broad range of construction materials, structural systems, and seismic performance levels that influence structural vulnerability. As summarised in Table 1, buildings are categorised based on primary construction materials, lateral load-resisting systems, seismic code levels, ductility levels, height (i.e., number of storeys), and occupancy type. Additional parameters are also incorporated to address regional or structural variations that can affect the seismic performance, such as the dominant inelastic mechanisms and floor type. Based on that, each building class is assigned a unique taxonomy string reflecting a combination of these attributes following GEM's taxonomy (Silva et al. 2022). For example, CR/LFM+CDH+DUM/H:3/RES represents a three-storey (H:3) reinforced concrete (CR) moment-resisting frame (LFM) with a high-code level (CDH), medium ductility (DUM), and residential (RES) occupancy. Further information on all building classes and their global distribution is provided in Yepes-Estrada et al. (2023).

Table 1. Building attributes used to define the building classes in the Global Vulnerability Database

Attribute	String	Details
Construction material	CR	Reinforced concrete
	EU	Earth construction
	INF	Informal construction
	MCF	Confined masonry
	MR	Reinforced masonry
	MUR	Unreinforced masonry
	MUR+ADO	Adobe construction
	MUR+CBH	Concrete block
	MUR+CLBRH	Hollow clay brick
	MUR+CLBRS	Solid clay brick
	MUR+STDRE	Dressed stone
	MUR+STRUB	Rubble stone
	S	Steel
	S+MCF	Steel and confined masonry
	SRC	Concrete composite with steel sections

	W	Timber
	W+WBB	Bamboo
	W+WWD	Wattle and daub
Lateral load-resisting system	LDUAL	Dual system
	LFINF	Infilled frame
	LMF	Moment frame
	LPB	Post and beam
	LWAL	Wall system
	LFBR	Braced frame
Code level	CDN	Pre-code
	CDL	Low code
	CDM	Moderate code
	CDH	High code
Ductility level	DNO	Non-ductile
	DUL	Low ductility
	DUM	Moderate ductility
	DUH	High ductility
Occupancy type	RES	Residential
	COM	Commercial
	IND	Industrial
Height	H:n	n is the number of storeys
Special attributes	NSCA	Non-structural components anchored
	VL100	100% loss of building volume (e.g., pancake collapse)
	CCA	Applicable to buildings in the Caribbean and Central America
	SOS	Soft-storey mechanism
	FC	Concrete floor
	FW	Wood floor
	RWO	Wood roof
	LC100	Lateral load coefficient 100%

The nonlinear behaviour of each building class is characterised via a capacity curve, which defines its global lateral (shear) strength and deformation capacity. This curve is usually transformed to the acceleration-displacement response spectrum domain, i.e., spectral displacement (SD) versus spectral acceleration (SA). Depending on the type of nonlinear behaviour of each building class, three idealised curve shapes are considered here:

- **Bilinear curves** for building classes without significant elastic stiffness degradation or post-yield loss of lateral strength (e.g., steel, timber frames).
- **Trilinear curves** for buildings with initial reduction of elastic stiffness due to cracking but relatively stable post-yield lateral strength (e.g., reinforced concrete bare frames, dual systems, unreinforced masonry).
- **Quadrilinear curves** for structures that undergo substantial reduction in lateral strength at large deformation levels (e.g., reinforced concrete infilled frames).

The three idealised shapes of capacity curves are shown in Figure 2, where SD_y and SA_y are the spectral displacement and acceleration at the yielding point, respectively, SD_u is the ultimate spectral displacement, T_1 is the first-mode vibration period, and T_y is the vibration period at the yielding point. The mathematical relationship between SA, SD, and T, used to define the capacity curve for each building class is given in Eq. (1).

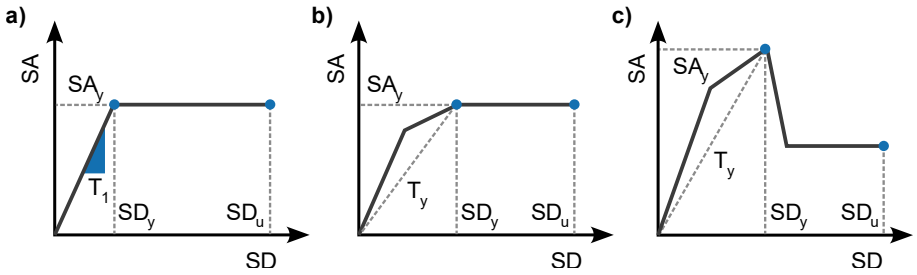

Figure 2. Idealised shapes of capacity curves: a) bilinear; b) trilinear; and c) quadrilinear.

$$SA = SD\left(\frac{2\pi}{T}\right)^2 \tag{1}$$

The vulnerability database of Martins and Silva (2021) provides capacity curves for nearly 500 building classes. In the present work, we expand the number of building classes to cover a wider range of construction materials, structural systems, heights, seismic code and ductility levels. The capacity curves of the new classes are defined based on results and findings from analytical and empirical studies in the literature, observations from experimental campaigns, and, where necessary, via engineering judgement from the authors and local experts that contributed throughout the years to the testing of the original database. The main references from which the capacity curves are sourced are outlined in Table 2.

Table 2. References for the capacity curves use to describe the nonlinear behaviour of different building classes

Primary Material of the Building Class	Literature references
Adobe and Rammed Earth	(Tarque et al. 2012; Villar-Vega et al. 2017a; Lang et al. 2018; Karanikoloudis and Lourenço 2018; Silveira et al. 2018; Battaglia et al. 2021)
Unreinforced Masonry	(Barbat et al. 2006; Borzi et al. 2008; Villar-Vega et al. 2017a; Lang et al. 2018)
Reinforced Masonry	(Voon and Ingham 2006; Shedid et al. 2008; Haach et al. 2010; Murcia-Delso and Shing 2012; Lotfy et al. 2022; FEMA 2024a)
Confined Masonry	(Magenes and Calvi 1992; Nucera et al. 2012; Erkoseoglu et al. 2014; Perez Gavilan et al. 2015; Villar-Vega et al. 2017a; Ahmed et al. 2018)
Reinforced Concrete	(Crowley et al. 2008; Bal et al. 2010; Ricci et al. 2011; Tischer et al. 2012; Villar-Vega et al. 2017a; Lang et al. 2018; Tarquini et al. 2019; Parra et al. 2019; Ugalde et al. 2019; Aljawhari et al. 2020; Suzuki and Iervolino 2020; Ugalde and Lopez-Garcia 2020; Farsangi et al. 2021; Gondaliya et al. 2023; FEMA 2024b; Nafeh and O'Reilly 2024)
Steel Structures	(Sabelli et al. 2003; McCormick et al. 2007; Tasnimi and Mohebkhah 2011; Ramirez et al. 2012; Radnić et al. 2013; Markulak et al. 2013; Abou-Elfath et al. 2017; Eladly 2017; Del Carpio R. et al. 2019; Jouneghani and Haghollahi 2020; FEMA 2024a)
Timber Structures	(Goda and Atkinson 2011; Loss et al. 2013; Villar-Vega et al. 2017b; Lang et al. 2018; FEMA 2024a)

The capacity curves from the studies in Table 2 serve as base prototypes, from which additional classes are derived by modifying the key parameters that vary with height. Specifically, for each base class, the T_y is first evaluated for the desired building height based on empirical formulae from the literature (e.g., Crowley and Pinho 2006). When such formulae are unavailable, T_y is assumed equal to $1.5T_1$ (Calvi et al. 2006). SD_u is then computed by scaling down the ultimate drift of the base class to account for

second-order effects (P-delta) at greater building heights, applying modification factors deduced from existing studies (FEMA 2012a; Crowley et al. 2021; Romão et al. 2021). Similarly, the yield drift is scaled to reflect its increase with building height and to estimate the corresponding SD_y. Finally, Eq. (1) is used to estimate the *SA* values and subsequently construct the full capacity curve for each newly defined building class. Additional ductility levels are considered by modifying the yield and ultimate drifts of the base class and then applying the same procedure. Figure 3 displays the counts of building classes, classified based on the primary construction material and height category. All values and assumptions for each capacity curve are available on the GitHub repository.

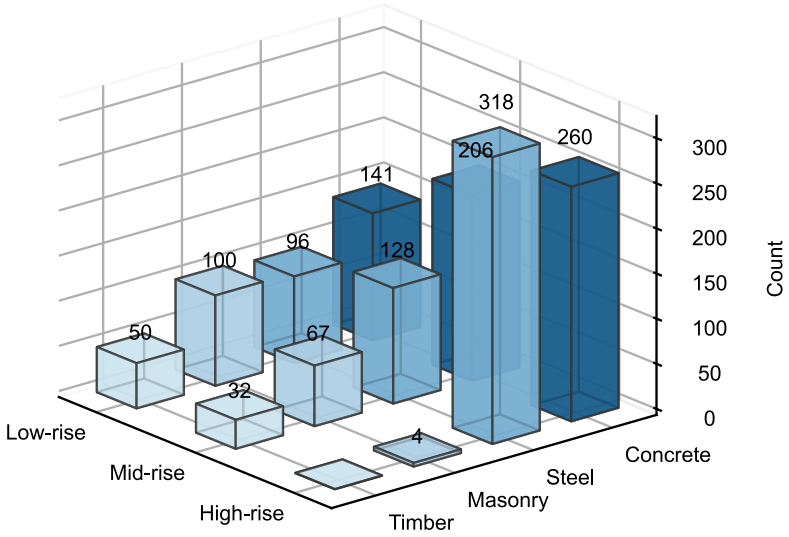

Figure 3. Building class counts based on primary construction material and height category.

2.2. Numerical Modelling Strategy

While Martins and Silva (2021) used SDOF models in the original vulnerability database, the new version adopts *stick-and-mass* MDOF systems with masses lumped at each floor level and connected by non-linear springs defining the storey-shear force versus drift behaviour (see Figure 4). These models explicitly capture storey-level demands like PSD and PFA, which are necessary to derive vulnerability functions for non-structural components and building contents, as described in Part II of this study. The new MDOF models also account for higher-mode effects and demand concentrations, offering a more realistic representation of structural response. Although these models do not simulate torsional modes and assume a shear-dominated storey response, previous studies have demonstrated their reliability and computational efficiency for regional and large-scale seismic risk applications (Lu et al. 2014; Gaetani d'Aragona et al. 2020).



Figure 4. Building class to stick-and-mass model idealisation.

To create the *stick-and-mass* MDOF systems for each building class, the capacity curves discussed in Section 2.1 are used as a starting point. While these capacity curves are generally sufficient to represent buildings as SDOF oscillators, their use in MDOF modelling requires conversion into pushover curves that describe the relationship between roof displacement (u_{roof}) and base shear (V_{base}). The conversion is based on the principles of structural dynamics as per Eqs. (2) and (3), where Γ_1 is the first-mode participation factor and m_{SDOF} is the effective mass of the SDOF oscillator, considered equal to 1.0 ton.

$$u_{roof} = SD\ \Gamma_1 \tag{2}$$

$$V_{base} = SA\ \Gamma_1\ m_{SDOF} \tag{3}$$

The storey mass of the MDOF (m_{MDOF}) model can now be computed via Eq. (4), derived on the basis that m_{SDOF} is equal to 1.0 ton. Here, $[I]$ denotes athe identity matrix of floor masses, with diagonal entries specifying the proportion of m_{MDOF} assigned to each floor. For instance, if all storey masses are equal, the diagonals of $[I]$ are set to 1.0. $\bar{J}$ is a unity vector of length equal to the number of storeys (n); ϕ_1 is the first-mode shape of the building; and ϕ_1^T is its transpose.

$$m_{MDOF} = \frac{\phi_1^T\ [I]\ \phi_1}{(\phi_1^T\ [I]\ \bar{J})^2} \tag{4}$$

The value of ϕ_1 is obtained through eigenvalue analysis, considering a uniform mass and stiffness across all storeys, except at the roof, where the mass is decreased by 25%. For buildings exhibiting soft-storey behaviour, the stiffness of the first storey is reduced by 80% to simulate the resulting demand concentration (Vijayanarayanan et al. 2017). For bare-frame structures without walls/infills, Eurocode 1-Part 4 (EN 1991-1-4 2004) recommends $\phi_{1,i} = (\mathrm{i}/n)^{0.6}$, where i is the storey number. The shear force-drift relationship can be finally proportioned for individual storeys based on ϕ_1, as expressed in Eqs. (5) and (6), following the formulation of Lu et al. (2014). V_i and Δ_i are the shear force and drift values associated with storey i; $\phi_{1,i}$ is the value of the first-mode shape at storey i out of n storeys. It is noted that Eqs. (2) to (6) assume that ϕ_1 is normalised such that its value at the roof is equal to 1.0.

$$V_i = \frac{\sum_{j=i}^{n} \phi_{1,i}\ m_i}{\sum_{k=1}^{n} \phi_{1,i}\ m_i}\ V_{base} \tag{5}$$

$$\Delta_i = \left(\phi_{1,i} - \phi_{1,i-1}\right) u_{roof} \tag{6}$$

Figure 5 presents illustrative examples of pushover curves for both SDOF and MDOF systems, along with storey-level $V_i - \Delta_i$ relationships used for MDOF modelling. The example compares two building classes: 1) a three-storey low-code reinforced concrete dual frame system with low ductility (CR/LDUAL/CDL+DUL/H:3); and 2) a three-storey moderate-code reinforced concrete infilled frame with low ductility (CR/LFINF/CDL+DUL/H:3).

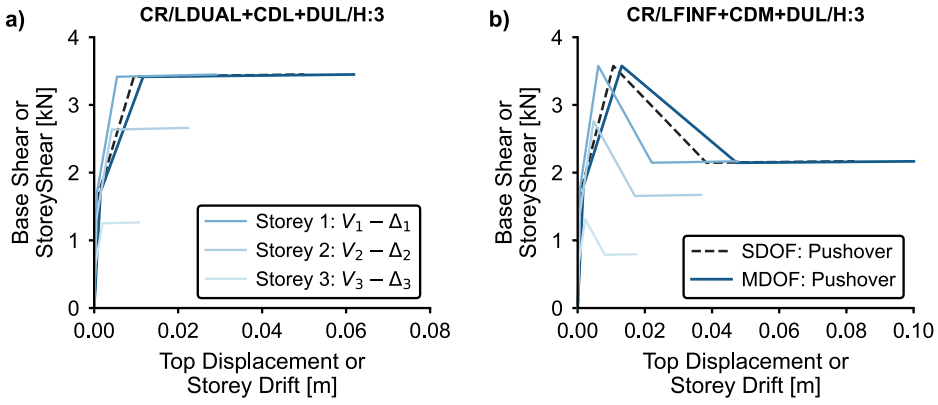

Figure 5. SDOF/MDOF pushover and storey-level V_i-Δ_i for: (a) three-storey low code reinforced concrete dual system with low ductility; and (b) three-storey moderate code reinforced concrete infilled frame with low ductility.

All MDOF systems are modelled using the OpenSeesPy (McKenna 2011) tool. Nonlinear springs connecting mass nodes are assigned the "*Pinching4*" material to reproduce the storey-level $V_i - \Delta_i$ relationships explained earlier. All models adopt Rayleigh damping (Zareian and Medina 2010; Gentile and Galasso 2021), with mass- and stiffness-proportional coefficients calibrated such that the first and second modes are damped via the ratios prescribed in Martins and Silva (2021) for each building class (i.e., 5% for reinforced concrete and timber, 7.5% for confined masonry, 10% for reinforced and unreinforced masonry, and 3% for steel structures).

2.3. Cloud Analysis and Ground-motion Selection

Deriving fragility and vulnerability functions typically requires conducting NLTHA to characterise the building's nonlinear dynamic response conditional on different ground-shaking intensity levels. Several methods exist in the literature, like the incremental dynamic (Vamvatsikos and Cornell 2002) and multiple stripe (Jalayer and Cornell 2009) analyses. This study adopts the cloud analysis approach (Jalayer et al. 2015), which subjects buildings to a set of typically unscaled ground-motion records. Cloud analysis is beneficial for regional risk assessments as it relies on "as-recorded" ground motions, thereby avoiding statistical biases due to scaling (Dávalos and Miranda 2019; Nafeh and O'Reilly 2022). It is also computationally efficient as it does not require selecting hazard-consistent, site-specific ground-motion sets, unlike multiple stripe analysis, for example.

This work advances the original vulnerability database of Martins and Silva (2021) by using a comprehensive, globally representative ground-motion dataset. From over 3,500 accelerograms, a subset of 700 records is selected, spanning over various tectonic regimes, including active shallow, stable continental, and subduction zones, which can influence ground shaking properties (e.g., duration, frequency content). The dataset integrates records from major databases: NGA-West (Bozorgnia et al. 2014), NGA-East (Goulet et al. 2021), NGA-Sub (Bozorgnia et al. 2022), KiK-Net (National Research Institute for Earth Science and Disaster Resilience 2019) and the Engineering Strong Motion Database (Luzi L. et al. 2020). The geographic distribution of the recording stations and tectonic regimes of the selected records are shown in Figure 6.

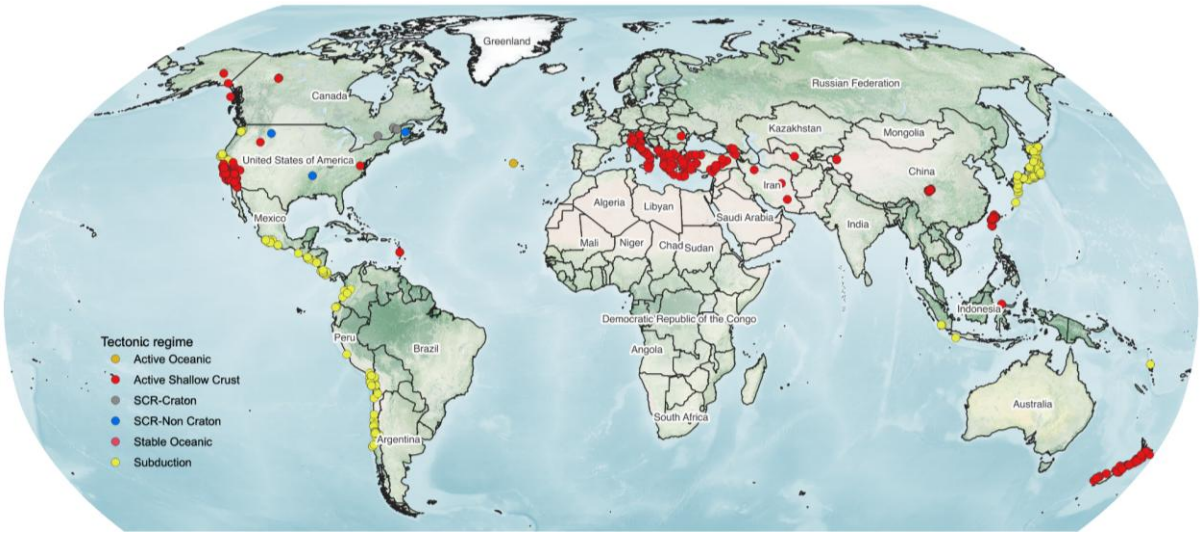

Figure 6. Geospatial locations and tectonic regimes of the recording stations

The ground-shaking intensity of the selected records is represented through several IMs tailored to the dynamic properties of the building classes. Specifically: 1) peak ground acceleration (PGA) for low-rise structures; 2) 5%-damped spectral acceleration, $SA(T)$, at 0.3s for some low- and mid-rise classes, *SA* at 0.6s for mid-rise classes, and *SA* at 1.0s for high-rise classes; and 3) average spectral acceleration (AvgSA) (e.g., Eads et al. 2015; Heresi and Miranda 2021; Aljawhari et al. 2025), defined as the geometric mean of ten equally-spaced SA values within a period range of 0.1s to 1.0s. Compared to

conventional IMs like $SA(T)$ or PGA, AvgSA has been shown to improve *efficiency*, *sufficiency*, and reduce bias in seismic response (e.g., O'Reilly 2021).

To ensure a sufficient coverage of a wide range of shaking intensities for NLTHA, the 3,500 records are distributed into equal acceleration bins for each IM type. A subset of 700 records is then randomly selected, subject to two constraints: 1) a minimum shaking intensity of 0.05g to ensure engineering relevance; and 2) at least ten records per bin. A small number of motions are scaled by factors not exceeding 2.5 to supplement the highest-intensity bins, ensuring sufficient damage observations in code-compliant building classes. Figure 7 depicts the distribution of ground-shaking intensities for the different IMs. The 5%-damped acceleration response spectra of individual ground-motion records and the corresponding mean spectrum are further illustrated in Figure 8. The compiled record set is available in the GitHub repository, along with the associated metadata.

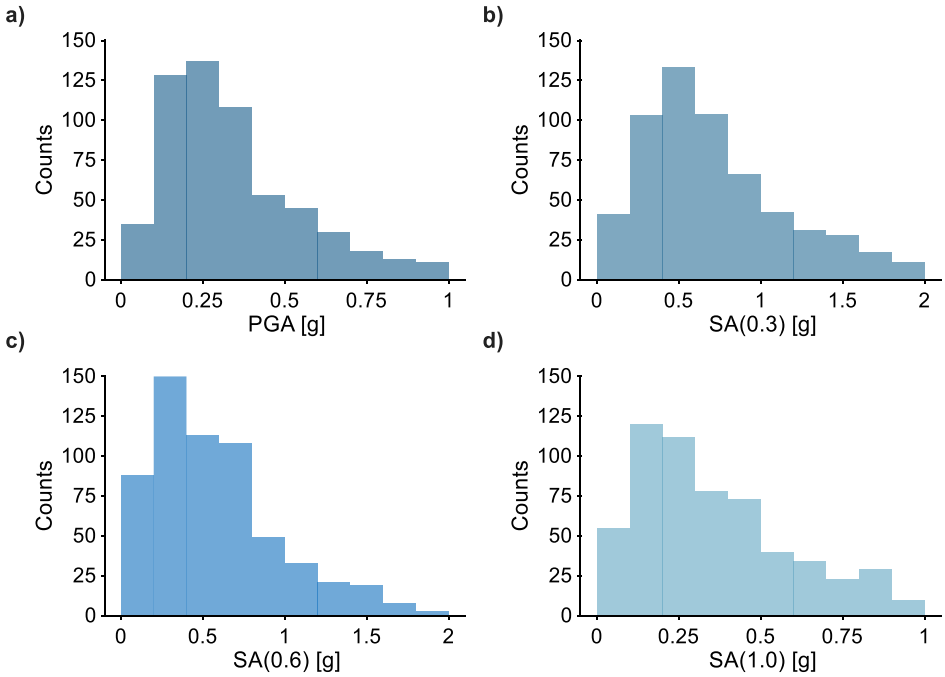

Figure 7. Ground-shaking intensity distribution for: a) PGA; b) $SA(0.3)$; c) $SA(0.6)$; and d) $SA(1.0)$.

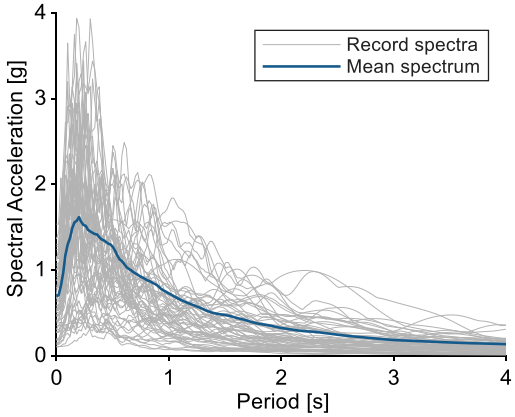

Figure 8. 5%-damped acceleration response spectra for individual records and the mean spectrum.

2.4. Definition of Damage States (DSs) and Fragility Derivation

Fragility functions for structural damage are derived in this study for each building class, defining the probability of exceeding a set of damage states, DSs, over a range of IM levels. Four DSs are considered here: slight (DS1), moderate (DS2), extensive (DS3), and complete (DS4). The onset of these DSs is inferred numerically through structural analysis, particularly when the building attains pre-defined

thresholds of a suitable engineering demand parameter (EDP). The selected EDP is the maximum interstorey drift ratio (θ_{max}) (e.g., Raghunandan et al. 2015; Aljawhari et al. 2022), which is strongly correlated with global structural damage, at least for drift-sensitive components.

In the original database of Martins and Silva (2021), the DS thresholds for SDOF oscillators were expressed in terms of SD within the capacity curves. Specifically, DS1 is marked at SD_y; DS2 at $0.67\ SD_y + 0.33\ SD_u$; DS3 at $0.33\ SD_y + 0.67\ SD_u$; and DS4 at SD_u. To adapt these thresholds to the MDOF framework, they are first converted into roof displacements, u_{roof}, for the corresponding *stick-and-mass* system. The interstorey drift profile at the onset of each DS is then derived using the principles of structural dynamics outlined in Section 2.2, from which the θ_{max} is obtained across all storeys. The transformation procedure is summarised in Table 3, where SD_y, SD_u, Γ_1, and $\phi_{1,i}$ are defined earlier, and h_i denotes the height of the i-th storey. This process is also illustrated in Figure 9.

Table 3. DS thresholds for MDOF systems expressed in terms of θ_{max}

Damage State	Maximum Interstorey Drift Ratio Thresholds
Slight (DS1)	$\theta_{max,DS1} = \max_{i=1,\dots,n_s} \left[\Gamma_1(\phi_{1,i} - \phi_{1,i-1})\ SD_y/h_i\right]$
Moderate (DS2)	$\theta_{max,DS2} = \max_{i=1,\dots,n_s} \left[\Gamma_1(\phi_{1,i} - \phi_{1,i-1})(0.67\ SD_y + 0.33\ SD_u)/h_i\right]$
Extensive (DS3)	$\theta_{max,DS3} = \max_{i=1,\dots,n_s} \left[\Gamma_1(\phi_{1,i} - \phi_{1,i-1})(0.33\ SD_y + 0.67\ SD_u)/h_i\right]$
Complete (DS4)	$\theta_{max,DS4} = \max_{i=1,\dots,n_s} \left[\Gamma_1(\phi_{1,i} - \phi_{1,i-1})\ SD_u/h_i\right]$

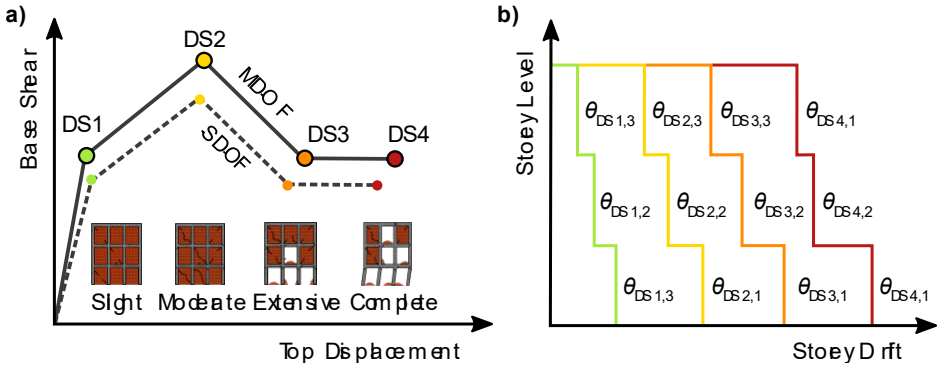

Figure 9. Derivation of DS thresholds for the MDOF systems: a) pushover results; b) interstorey drift profile

The fragility functions are derived using cloud analysis, which adopts NLTHA to produce a dataset of ground-shaking IM versus EDP pairs. A probabilistic seismic demand model is then fitted to this dataset in the form of a power-law relation, as per Eq. (7), where $E[EDP]$ is the expected EDP value and a and b are regression parameters (see Figure 10). The dispersion (β_{rec}) reflecting the record-to-record response variability is given in Eq. (8). k is the number of ground motions, and EDP_i is the EDP produced by record i. To account for the additional uncertainty due to the building-to-building variability (and modelling assumptions), an extra dispersion term (β_{bldg}) is included here, taken as 0.30 following previous studies (e.g., FEMA 2012b). The total dispersion (β) is therefore expressed as per Eq. (9).

$$E[EDP] = a\ IM^b \tag{7}$$

$$\beta_{rec} = \sqrt{\frac{\sum_{i=1}^{k} \ln EDP_i - E[\ln EDP]}{k-2}} \tag{8}$$

$$\beta = \sqrt{{\beta_{rec}}^2 + {\beta_{bldg}}^2} \tag{9}$$

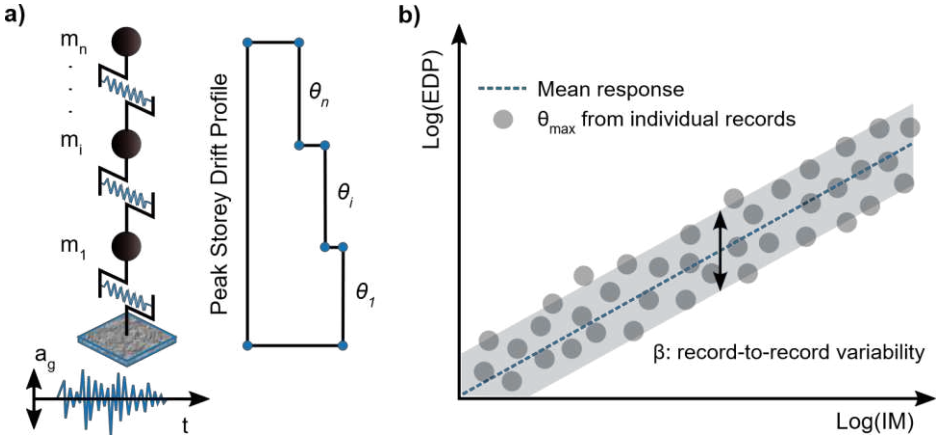

Figure 10. a) Idealised *stick-and-mass* MDOF model with PSD demands evaluated via NLTHA; and b) cloud analysis with fitted probabilistic seismic demand model.

To estimate the regression parameters a and b of the power-law in Eq. (7), the Maximum Likelihood Method (Stafford 2008; Lallemant et al. 2015) is used, which estimates the values of these parameters that maximise the probability of observing the NLTHA results (i.e., EDP_i), given the corresponding IM values, as per Eq. (10). ϕ is the probability density function of the standard normal distribution.

$$L = \prod_{i=1}^{k} \left[\phi \left(\frac{EDP_i - a - bIM_i}{\beta} \right) \right] \tag{10}$$

Although straightforward in principle, fitting the power law using the above procedure can be biased due to extreme NLTHA outcomes (i.e., unusually large drifts or accelerations due to numerical instability typically caused by collapse). Including such outliers in the regression might distort fitted parameters and exaggerate the predicted damage, especially at high IM levels. To address this challenge, a "censored" regression procedure is adopted, with a censoring threshold, EDP_c, defined as 1.5 times the EDP associated with DS4 (Martins and Silva 2021). Any observation exceeding this limit is treated as censored, i.e., the building is assumed to have collapsed. Accordingly, analysis results are split into n_0 uncensored and n_c censored observations. For the uncensored subset, the likelihood function follows Eq. (10), whereas for the censored one, the contribution is expressed through the complementary probability of exceeding EDP_c. The combined log-likelihood function is given in Eq. (11) (Stafford 2008), where Φ is the cumulative distribution function of the standard normal distribution.

$$\ln(L) = \sum_{i=1}^{n_0} \ln \phi \left(\frac{EDP_i - a - bIM_i}{\beta} \right) + \sum_{j=1}^{n_c} \ln \left[1 - \Phi \left(\frac{EDP_c - a - bIM_j}{\beta} \right) \right] \tag{11}$$

Once the power-law model is fitted, fragility functions for all DSs can be derived. These functions are mathematically expressed as a lognormal cumulative distribution function (Porter et al. 2007; Eads et al. 2013), as per Eq. (12), which provides the probability that a particular DS is exceeded, given an IM. μ_{DSi} is the median IM level at which the "i-th" DS is reached (DSi). β and Φ were defined previously.

$$P(DS \geq DSi|IM) = \Phi \left(\frac{ln(IM/\mu_{DSi})}{\beta} \right) \tag{12}$$

2.5. Derivation of Vulnerability Functions

Vulnerability functions quantify the economic loss ratio over a range of IM values, which represents the repair cost of damaged structural components normalised by their replacement cost. These functions can be generated by combining the probabilities of different DSs, obtained from the fragility functions (Section 2.4), with adequate damage-to-loss ratios via the total probability theorem, according to Eq. (13).

$$E(LR|IM) = \sum_{i=1}^{n_{DS}} P(DS = DSi|IM)\, DLR_{DSi} \tag{13}$$

Where $E(LR|IM)$ is the expected structural loss ratio conditioned on an IM level, $P(DS = DSi|IM)$ is the probability that DS is equal to DSi, given the IM level; DLR_{DSi} is the damage-to-loss ratio associated with DSi; and n_{DS} is the number of DSs. The variability of $E(LR|IM)$ is captured using the method proposed by Silva (Silva 2019), who examined the influence of record-to-record variability on the dispersion of loss ratios for different building classes. The selected DLR_{DSi} values are consistent with those available in the literature, derived using either empirical data (e.g., Di Pasquale et al. 2005; Bal et al. 2008) or analytical procedures (e.g., Martins et al. 2016; Aljawhari et al. 2023, 2025). Table 4 provides the mean DLR_{DSi} for each DS.

Table 4: Selected damage-to-loss ratios for each DS

Damage State	Mean damage-to-loss ratio
Slight (DS1)	0.05
Moderate (DS2)	0.15
Extensive (DS3)	0.60
Complete (DS4)	1.00

2.6. Integration with the OQ-VMTK Package

The numerical modelling and analysis workflows presented herein are fully automated through the new version of the OpenQuake's Vulnerability Modellers Toolkit" (OQ-VMTK), an open-source Python package that imports and transforms SDOF capacity-curve information into the corresponding *stick-and-mass* MDOF system. The toolkit streamlines essential modelling tasks, including the assignment of nodes, masses, boundary conditions, nonlinear springs, and damping, as well as the execution of various analysis types (e.g., gravity, modal, non-linear static, non-linear cyclic, and NLTHA using user-specified records). The OQ-VMTK further incorporates modules that automate the derivation of fragility functions adopting different methods, in addition to vulnerability functions for a wide range of seismic consequences (e.g., economic losses in structural and non-structural components, content losses, fatalities, collapses). High-quality data visualisation is also supported through a dedicated module. The OQ-VMTK is freely accessible on GitHub[2], thus allowing the scientific community to reproduce the models and results described in this study, as well as to build models for building classes not yet covered by this study. Users are referred to Nafeh et al. (2026) for a detailed description of the OQ-VMTK.

3. END-TO-END APPLICATION: RESULTS AND DISCUSSION

3.1. Sample Fragility and Vulnerability Functions

Given the large number of building classes analysed in this study, only selected results are reported here to highlight key insights. The complete results and datasets are accessible via GitHub[3]. Table 5 summarises the parameters of the derived structural fragility functions (median, μ_{DSi}, and dispersion, β) for common building classes worldwide. These differ in height (H) and include reinforced concrete frames with masonry infills (CR/LFINF), several unreinforced masonry (MUR) typologies, and steel frames with shear walls (S/LWAL). For each class, the most efficient IM is selected, defined as the one minimising record-to-record variability (i.e., lowest β_{rec} value).

Clear trends are observed across design code levels and ductility classes. Buildings designed to high code (CDH) and high ductility (DUH) exhibit μ_{DSi} values up to twice those of low-code (CDL) and low ductility (DUL) counterparts. The influence of primary construction material and lateral load-resisting system is also evident: S/LWAL buildings display the largest μ_{DSi} values and are therefore the

[2] https://github.com/GEMScienceTools/oq-vmtk

least susceptible to seismic damage. For CR/LFINF frames, the μ_{DSi} values are consistently higher than for MUR buildings, especially for the more severe DS levels.

Table 5. Parameters of structural fragility functions: median (μ_{DSi}) and dispersion (β)

Building class	Efficient IM	μ_{DS1} [g]	μ_{DS2} [g]	μ_{DS3} [g]	μ_{DS4} [g]	β
CR/LFINF+CDH+DUH/H:3	SA(0.6s)	0.316	0.850	1.308	1.712	0.682
CR/LFINF+CDH+DUM/H:3	SA(0.6s)	0.287	0.723	1.089	1.408	0.651
CR/LFINF+CDH+DUL/H:3	SA(0.6s)	0.276	0.726	1.109	1.446	0.648
CR/LFINF+CDM+DUM/H:3	SA(0.6s)	0.231	0.551	0.810	1.030	0.620
CR/LFINF+CDM+DUL/H:3	SA(0.6s)	0.187	0.437	0.644	0.822	0.604
CR/LFINF+CDL+DUL/H:3	SA(0.6s)	0.140	0.343	0.510	0.654	0.548
CR/LFINF+CDN+DNO/H:3	SA(0.6s)	0.129	0.302	0.444	0.567	0.537
CR/LFINF+CDH+DUH/H:8	SA(1.0s)	0.187	0.369	0.532	0.676	0.606
CR/LFINF+CDH+DUM/H:8	SA(1.0s)	0.171	0.327	0.465	0.587	0.581
CR/LFINF+CDH+DUL/H:8	SA(1.0s)	0.161	0.314	0.450	0.570	0.569
CR/LFINF+CDM+DUM/H:8	SA(1.0s)	0.142	0.266	0.373	0.467	0.563
CR/LFINF+CDM+DUL/H:8	SA(1.0s)	0.116	0.198	0.271	0.335	0.529
CR/LFINF+CDL+DUL/H:8	SA(1.0s)	0.081	0.142	0.196	0.243	0.516
CR/LFINF+CDN+DNO/H:8	SA(1.0s)	0.073	0.121	0.163	0.201	0.505
S/LWAL+CDH+DUH/H:7	SA(0.3s)	1.503	2.713	3.743	4.633	0.644
S/LWAL+CDH+DUM/H:7	SA(0.6s)	0.577	1.131	1.633	2.084	0.712
S/LWAL+CDM+DUM/H:7	SA(0.6s)	0.525	0.889	1.228	1.536	0.646
S/LWAL+CDM+DUL/H:7	SA(0.6s)	0.428	0.641	0.839	1.017	0.628
S/LWAL+CDL+DUM/H:7	SA(0.6s)	0.404	0.540	0.671	0.790	0.643
S/LWAL+CDL+DUL/H:7	SA(0.6s)	0.324	0.428	0.525	0.611	0.581
MUR+CBH/LWAL+DNO/H:3	SA(0.6s)	0.254	0.470	0.666	0.842	0.583
MUR+STDRE/LWAL+DNO/H:3	SA(0.6s)	0.225	0.408	0.574	0.724	0.590
MUR+CLBRS/LWAL+DNO/H:3	Sa(0.6s)	0.204	0.366	0.508	0.632	0.587
MUR+CLBRH/LWAL+DNO/H:3	Sa(0.6s)	0.188	0.343	0.480	0.601	0.588
MUR+STRUB/LWAL+DNO/H:3	Sa(0.6s)	0.186	0.331	0.460	0.575	0.595
MUR+ADO/LWAL+DNO/H:3	Sa(0.6s)	0.157	0.260	0.352	0.433	0.501

To illustrate some of the above trends, Figure 11 presents structural fragility functions for a four-storey reinforced concrete frame with masonry infills, in moderate-code/low-ductility (Figure 11a) and high-code/moderate-ductility (Figure 11b) configurations. Figure 11(c-d) show similar functions for four-storey unreinforced masonry buildings, one with rubble stone (Figure 11c) and the other with hollow concrete blocks (Figure 11d). The efficient IM and building height are matched across the selected classes to enable a direct comparison of their fragility characteristics and functions. The associated vulnerability functions are depicted in Figure 12, further confirming the differences among the four building classes with respect to structural losses.

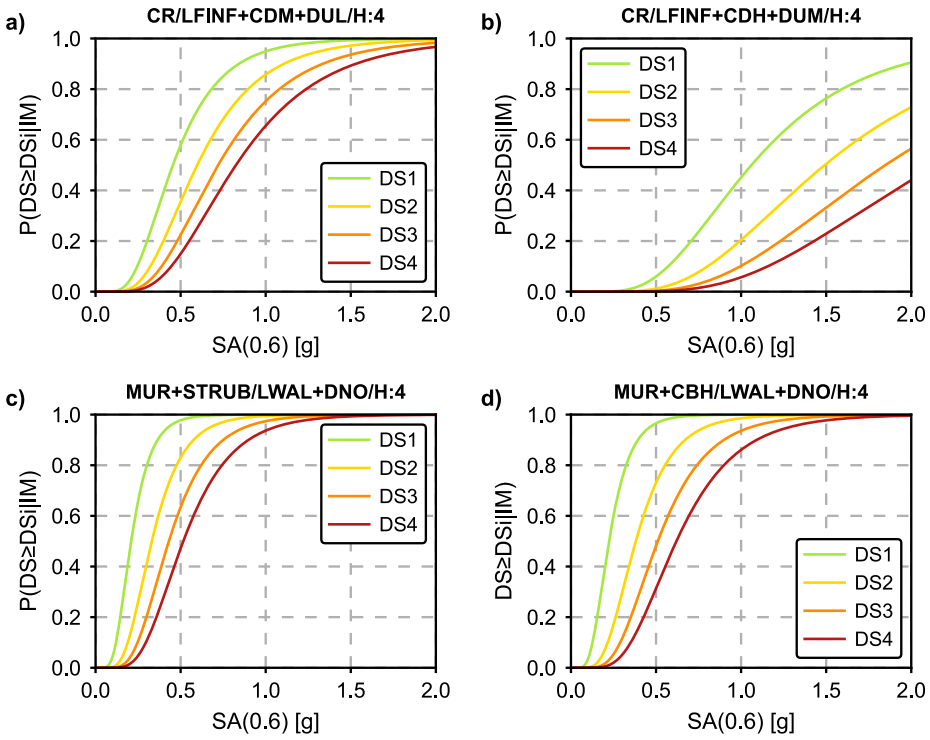

Figure 11. Fragility functions for: a) four-storey reinforced concrete infilled frame with moderate-code/low-ductility; b) four-storey reinforced concrete infilled frame with high-code/moderate-ductility; (c) four-storey pre-code unreinforced masonry with rubble stone; and d) four-storey pre-code unreinforced masonry with concrete blocks

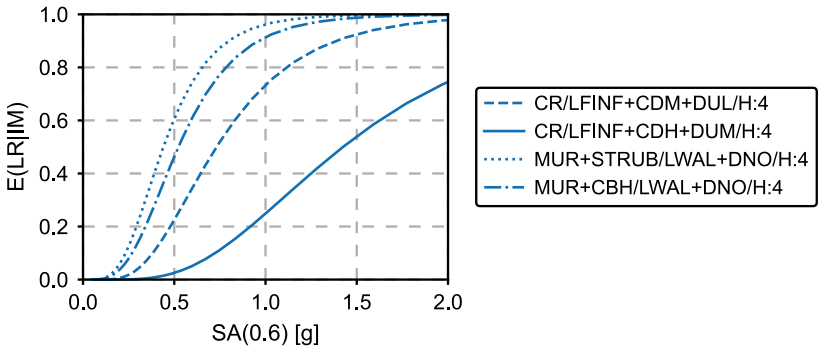

Figure 12. Vulnerability functions for selected building classes

3.2. Original versus New Global Vulnerability Database

The new global vulnerability database introduced in this study brings major upgrades over the original version of Martins and Silva (2021). Key improvements include the transition of numerical modelling from simplified SDOF oscillators to stick-and-mass MDOF systems and the adoption of θ_{max} as the primary EDP to assess structural damage. Compared to SD, which was used for SDOF oscillators, θ_{max} better captures variation in deformation patterns and thus provides a more realistic characterisation of multi-storey building response. These upgrades provide a more reliable representation of seismic fragility and vulnerability, especially for building classes with response patterns that cannot be effectively addressed by SDOF oscillators. This section compares the new and the original databases with respect to fragility and vulnerability to highlight potential implications on regional risk assessments.

Figure 13 compares the median values of fragility functions, μ_{DSi}, across different building height ranges. In each plot, the horizontal axis represents values from the new database, while the vertical axis shows those from Martins and Silva (2021). For one-storey buildings (Figure 13a), which are modelled as SDOF oscillators in both databases, the results differ slightly by an average of 15%, mainly reflecting

the impact of the newly compiled ground-motion set. For low- to mid-rise buildings up to eight storeys (Figure 13b), deviations increase with an average difference in μ_{DSi} up to 30%, due to both the updated modelling strategy and the expanded record set. These observations suggest a limited impact on regional risk assessment outcomes, though MDOF models tend to predict larger losses for multi-storey buildings. By contrast, significant discrepancies are observed for high-rise buildings between 8 and 20 storeys (Figure 13c). In fact, values from the original database are on average 50% larger than those derived in this study. This stems from the inability of SDOF oscillators to capture higher-mode effects and localised inter-storey demands, which can amplify deformations and increase damage. Consequently, reliance on SDOF models may lead to large risk underestimations for high-rise buildings

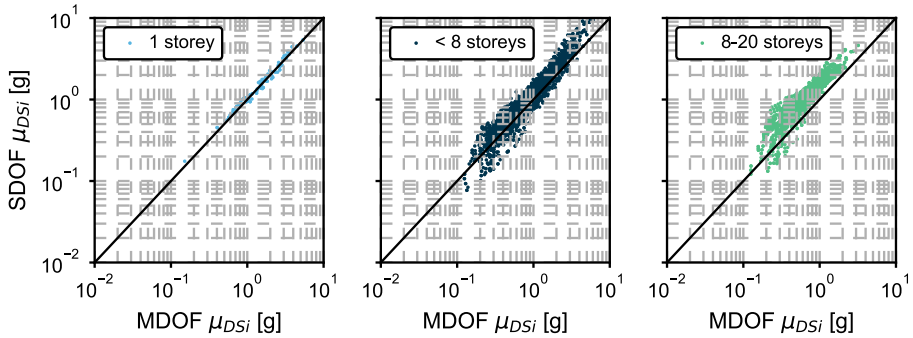

Figure 13. Comparing the new and original databases in terms of median values, μ_{DSi}, of structural building-level fragility relationships for these height ranges: a) one-storey; b) up to 8 storeys; and c) 8-20 storeys

The above trends are also illustrated in Figure 14, which compares structural vulnerability functions for mid-rise (8 storeys) and high-rise (35 storeys) reinforced concrete dual systems, both with moderate code and low ductility. For the mid-rise class in Figure 14(a), the functions from both databases show close agreement. On the contrary, Figure 14(b) reveals that for the selected high-rise building class, the loss ratios, LR, predicted by the MDOF-based vulnerability function could reach up to 2.5 times higher than those calculated through the SDOF model.

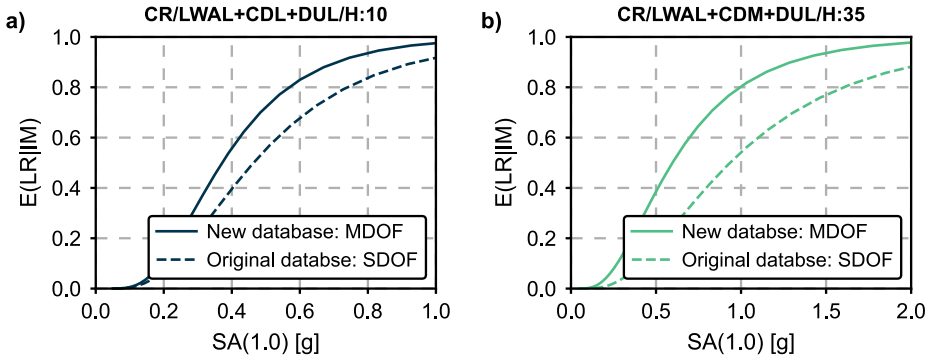

Figure 14. Structural vulnerability functions from the new and original databases for reinforced concrete dual system with moderate code and low ductility: (a) 5 storeys; and (b) 35 storeys

To further demonstrate the influence of the new modelling strategy and ground-motion set on risk-related applications, average annual loss ratios ($AALR$) are evaluated for a sample of low-, mid-, and high-rise building classes, selected based on their predominance in the global exposure model (Yepes-Estrada et al. 2023). The $AALR$ reflects the expected yearly repair costs of a building (normalised by its replacement cost) averaged over the full range of possible ground-shaking scenarios. The $AALR$ is often used by policymakers, insurers, and engineers to prioritise retrofitting strategies, allocate resources, and evaluate the cost-effectiveness of risk-reduction measures.

The $AALR$ is practically derived here by combining the vulnerability function with a hazard curve defining the mean annual frequency of exceeding (λ) different ground-shaking levels (e.g., Gentile and Galasso

2022). The convolution produces a loss curve, which relates λ to different levels of LR. The area under this curve, obtained via integration, gives the $AALR$, as expressed in Eq. (14).

$$AALR = \int_0^{\infty} LR(\lambda)\, d\lambda \tag{14}$$

Three cities with high seismic activity are adopted as test beds: Wellington (New Zealand), Istanbul (Türkiye), and Los Angeles (USA). The hazard curves for these locations accounting for the different IM types are acquired from GEM's hazard mosaic (Johnson et al. 2023). Figure 15 depicts all the hazard curves, assuming rock site conditions.

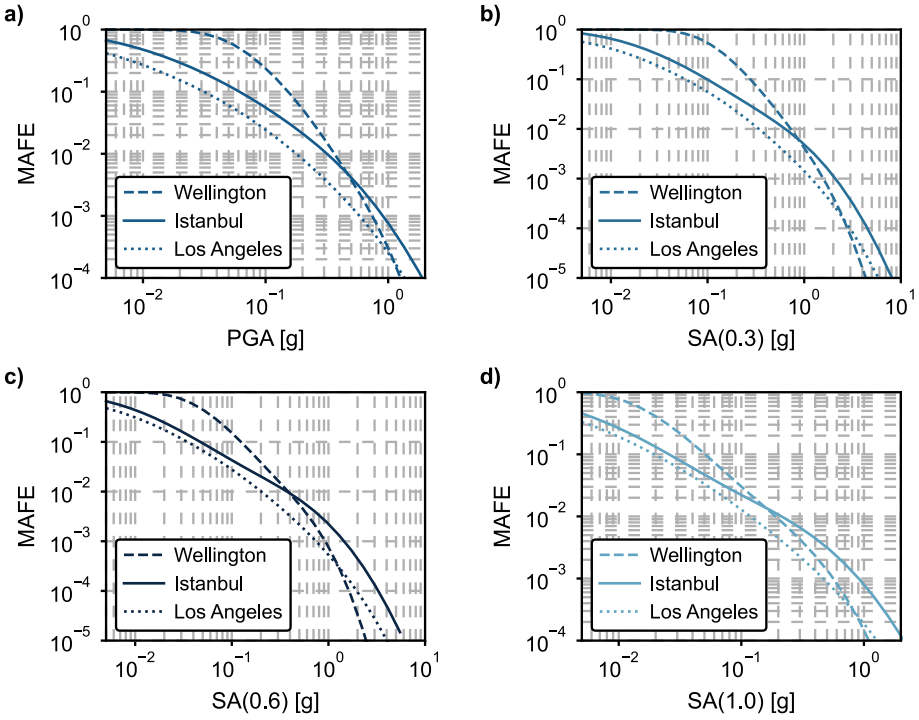

Figure 15. Hazard curves of PGA for Wellington, Istanbul, and Los Angeles, considering the following IMs: a) PGA; b) $SA(0.3)$; c) $SA(0.6)$; and d) $SA(1.0)$.

Figure 16 displays the $AALR$ values for the selected low- and mid-rise building classes (< 8 storeys), considering both the MDOF- and SDOF-based vulnerability functions. The two databases show a close agreement, and variations remain minor across most of the selected building classes, with an average difference percentage ranging between 9% and 26%. This range does not only depend on the building class, but also the hazard curve, especially that the efficient IM can differ when comparing the two modelling strategies. Generally, the AALR values derived from MDOF-based vulnerability tend to be relatively larger for multi-storey building classes, echoing the findings extrapolated from Figure 13.

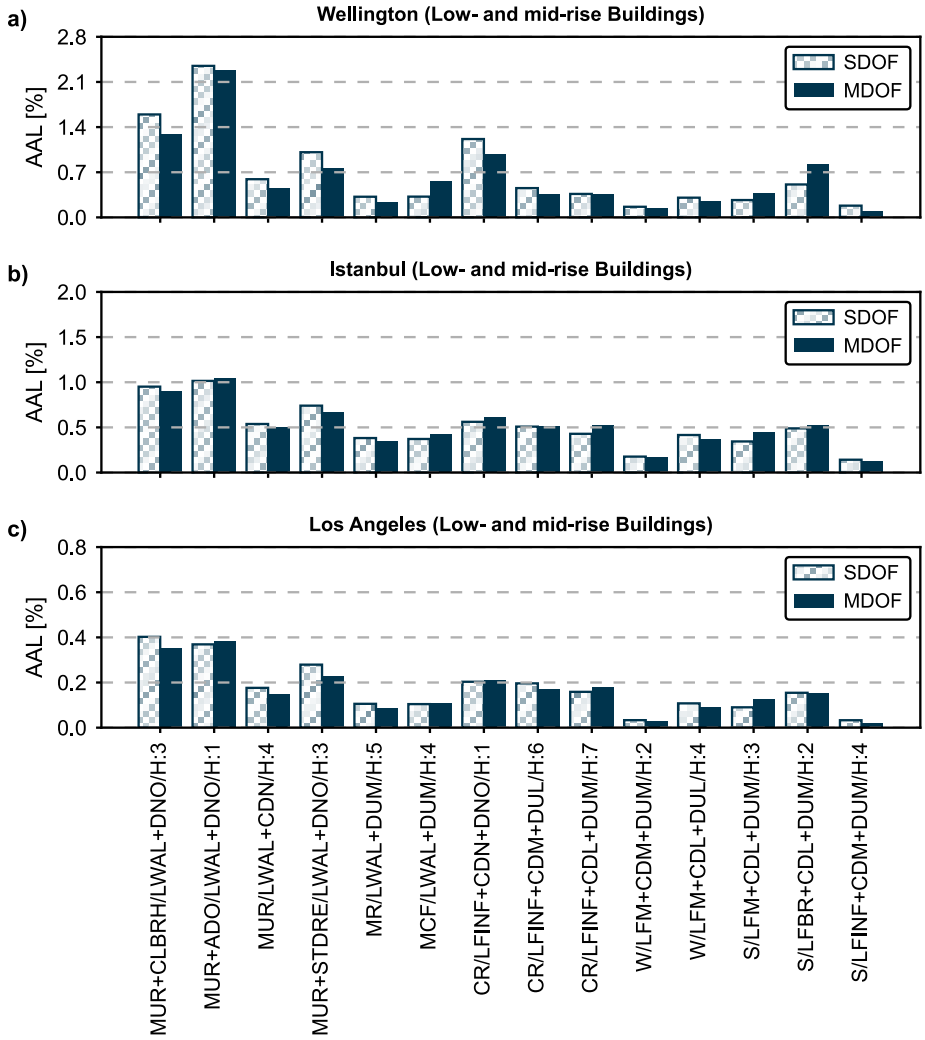

Figure 16. Average annual loss, AAL, for low- and mid-rise building classes located in: a) Bucharest; b) Istanbul; and c) Los Angeles

A similar exercise is also carried out for the sample of high-rise building classes with vertical heights exceeding 8 storeys. The resulting *AALR* values are illustrated in Figure 17, revealing a consistent underestimation of economic losses when using SDOF-based vulnerability functions to estimate *AALR*. In fact, the updated modelling strategy raises the average difference percentage between the MDOF-based and SDOF-based *AALR* values to between 70% and 98%, depending on the building class and the corresponding hazard curve (i.e., city). This finding indicates that seismically active countries with a large stock of high-rise structures can witness a considerable increase in seismic risk predictions at regional level. These results highlight the substantial impact of modelling choices on the reliability of loss analysis and risk assessment outcomes, demonstrating that simplified representations may considerably bias our regional predictions and, consequently, the decision-making process.

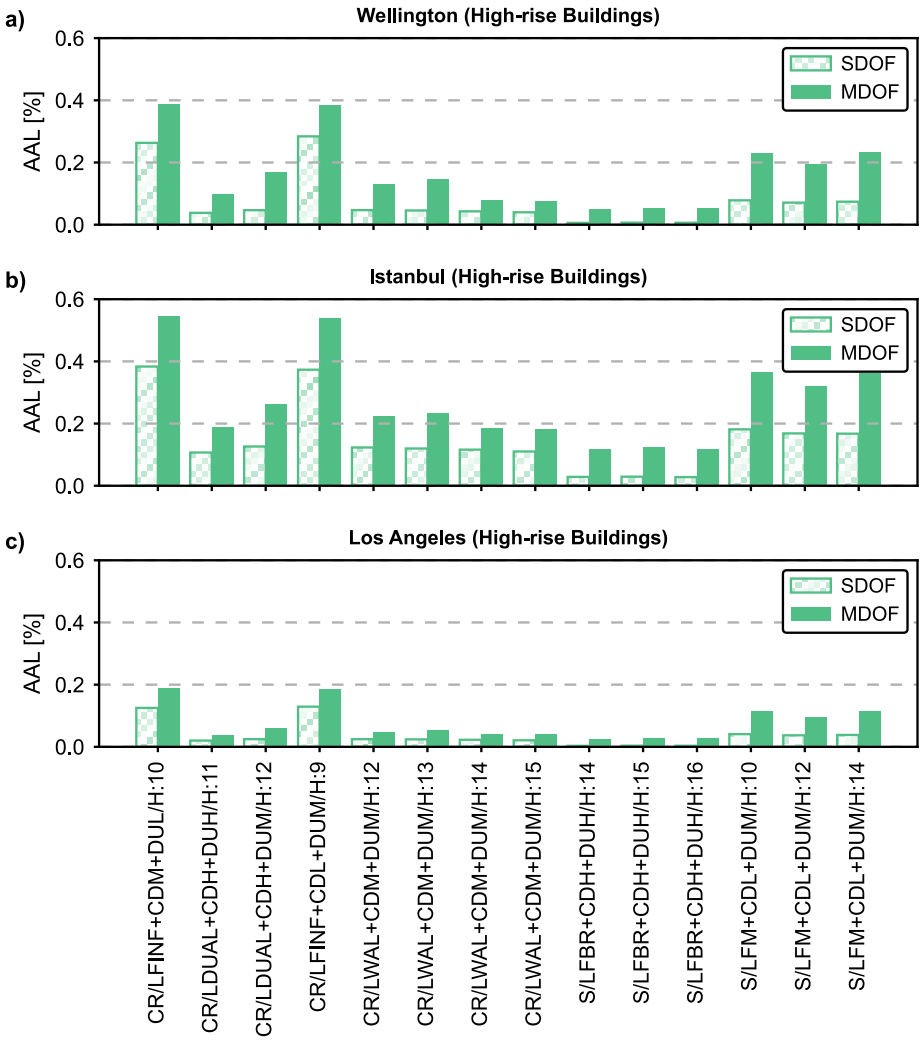

Figure 17. Average annual loss, AAL, for high-rise building classes located in: a) Bucharest; b) Istanbul; and c) Los Angeles

4. CONCLUSIONS

This study developed the most comprehensive global seismic vulnerability database to date, delivering detailed fragility and vulnerability information, specifically tailored for large-scale regional risk assessment applications. This database offers reliable simulations of seismic response across a broad spectrum of building classes via a refined numerical modelling strategy. Leveraging the earlier version of the database by Martins and Silva (2021), the new global vulnerability database enables more robust risk assessments and supports effective disaster mitigation planning through the following key innovations:

- An extensive range of more than 1,400 different building classes, encompassing a wide range of construction materials, lateral load-resisting systems, code levels, ductility levels, and heights.
- An advanced numerical modelling strategy, which transforms the simplified SDOF systems in the original database to *stick-and-mass* MDOF oscillators. These models explicitly capture both storey-level demands (e.g., storey drift, peak floor acceleration) and complex seismic response patterns (e.g., soft storey, higher modes), allowing a better characterisation of damage and loss.
- An extended ground-motion records set for NLTHA, covering several tectonic settings (e.g., subduction, stable continental) and IMs.
- A new suite of fragility relationships and vulnerability functions for structural damage and loss, respectively, was derived based on the new MDOF systems.

A comparison between the new vulnerability database and the original one by Martins and Silva (Martins and Silva 2021) revealed a high consistency in median values of structural fragility relationships, μ_{DSi}, for low- and mid-rise structures (up to 8 storeys). In contrast, for high-rise buildings, the original database substantially overestimated the μ_{DSi} values by even 50% in some building classes, as SDOF systems cannot capture higher-mode effects, which often result in larger deformation. Consequently, structural losses in high-rise buildings are likely underestimated in the original database.

Future improvements may include tectonic-specific fragility and vulnerability data (e.g., subduction zones, strike-slip faults); state-dependent fragility and vulnerability data that consider the influence of sequential ground shaking and damage accumulation; refining building contents vulnerability for buildings where content loss can significantly impact recovery, like hospitals, manufacturing plants, and data centres; and addressing the effects of structural retrofitting.

This work presented here constitutes the first part of the new Global Vulnerability Model, which will be used for the development of the 2026 version of the Global Seismic Risk Model. A companion paper (Part II) uses this work as a basis to address further seismic consequences, particularly damage and loss in non-structural components and building contents.

STATEMENTS & DECLARATIONS

Funding

The authors declare that no funds, grants, or other support were received during the preparation of this manuscript.

Competing Interests

The authors have no relevant financial or non-financial interests to disclose.

Author Contributions

All authors contributed to the study conception and design. Material preparation, literature review, modelling, analysis, post-processing, and figures design were performed by KA and AN. All authors contributed to the writing and revision of the manuscript.

Data Availability

The datasets generated during the current study are available in our GitHub repository, https://github.com/gem/global_vulnerability_model/tree/v2025.0.0

REFERENCES

Abou-Elfath H, Ramadan M, Meshaly M, Fdiel HA (2017) Seismic performance of steel frames designed using different allowable story drift limits. Alexandria Engineering Journal 56:241–249. https://doi.org/10.1016/j.aej.2016.08.028

Ahmed A, Ahmad I, Shahzada K, et al (2018) Seismic Capacity Assessment of Confined Brick Masonry Building: An Experimental Approach. Shock and Vibration 2018:. https://doi.org/10.1155/2018/4756352

Aljawhari K, Gentile R, Freddi F, Galasso C (2020) Effects of ground-motion sequences on fragility and vulnerability of case-study reinforced concrete frames. Bulletin of Earthquake Engineering. https://doi.org/10.1007/s10518-020-01006-8

Aljawhari K, Gentile R, Galasso C (2024) Earthquake-induced environmental impacts for residential Italian buildings: Consequence models and risk assessment. Journal of Building Engineering 84:. https://doi.org/10.1016/j.jobe.2023.108149

Aljawhari K, Gentile R, Galasso C (2025) Beyond Direct Economic Losses: An Integrated Approach to Seismic Retrofit Considering Sustainability and Indirect Losses. Earthq Eng Struct Dyn. https://doi.org/10.1002/eqe.4324

Aljawhari K, Gentile R, Galasso C (2022) A fragility-oriented approach for seismic retrofit design. Earthquake Spectra 38:1813–1843. https://doi.org/10.1177/87552930221078324

Aljawhari K, Gentile R, Galasso C (2023) Simulation-based consequence models of seismic direct loss and repair time for archetype reinforced concrete frames. Soil Dynamics and Earthquake Engineering 172:107979. https://doi.org/10.1016/j.soildyn.2023.107979

Angelucci G, Mollaioli F, Molle M, Paris S (2022) Performance assessment of Timber High-rise Buildings: Structural and Technological Considerations. The Open Construction & Building Technology Journal 16:. https://doi.org/10.2174/18748368-v16-e2206270

Bal IE, Crowley H, Pinho R, Gülay FG (2008) Detailed assessment of structural characteristics of Turkish RC building stock for loss assessment models. Soil Dynamics and Earthquake Engineering 28:914–932. https://doi.org/10.1016/j.soildyn.2007.10.005

Bal IEngin, Crowley Helen, Pinho Rui (2010) Displacement-based earthquake loss assessment : method development and application to Turkish building stock. IUSS Press

Barbat AH, Pujades LG, Lantada N (2006) Performance of Buildings under Earthquakes in Barcelona, Spain. Computer-Aided Civil and Infrastructure Engineering 21:573–593. https://doi.org/10.1111/j.1467-8667.2006.00450.x

Battaglia L, Ferreira TM, Lourenço PB (2021) Seismic fragility assessment of masonry building aggregates: A case study in the old city Centre of Seixal, Portugal. Earthq Eng Struct Dyn 50:1358–1377. https://doi.org/10.1002/eqe.3405

Borzi B, Crowley H, Pinho R (2008) Simplified Pushover-Based Earthquake Loss Assessment (SP-BELA) Method for Masonry Buildings. International Journal of Architectural Heritage 2:353–376. https://doi.org/10.1080/15583050701828178

Bozorgnia Y, Abrahamson NA, Ahdi SK, et al (2022) NGA-Subduction research program. Earthquake Spectra 38:783–798. https://doi.org/10.1177/87552930211056081

Bozorgnia Y, Abrahamson NA, Atik L Al, et al (2014) NGA-West2 Research Project. Earthquake Spectra 30:973–987. https://doi.org/10.1193/072113EQS209M

Bull D (2013) Earthquakes and the effects on structures: Some of the lessons learnt. Australian Journal of Structural Engineering 14:. https://doi.org/10.7158/S12-034.2013.14.2

Calvi GM, Pinho R, Crowley H (2006) State-of-the-knowledge on the period elongation of RC buildings during strong ground shaking. In: 1st European Conference on Earthquake Engineering and Seismology. Geneva

Cornell CA, Asce M, Jalayer F, et al (2002) Management Agency Steel Moment Frame Guidelines. 526–533

Crowley H, Borzi B, Pinho R, et al (2008) Comparison of Two Mechanics-Based Methods for Simplified Structural Analysis in Vulnerability Assessment. Advances in Civil Engineering 2008:1–19. https://doi.org/10.1155/2008/438379

Crowley H, Pinho R (2006) Simplified Equations for Estimating the Period of Vibration of Existing Buildings. In: 1st European Conference on Earthquake Engineering and Seismology. Geneva

Crowley H, Silva V, Martins L, et al (2021) OPEN MODELS AND SOFTWARE FOR ASSESSING THE VULNERABILITY OF THE EUROPEAN BUILDING STOCK. pp 2678–2688

Dávalos H, Miranda E (2019) Evaluation of bias on the probability of collapse from amplitude scaling using spectral-shape-matched records. Earthq Eng Struct Dyn 48:970–986. https://doi.org/10.1002/eqe.3172

Del Carpio R. M, Mosqueda G, Lignos DG (2019) Experimental investigation of steel building gravity framing systems under strong earthquake shaking. Soil Dynamics and Earthquake Engineering 116:230–241. https://doi.org/10.1016/j.soildyn.2018.10.017

Di Pasquale G, Orsini G, Romeo RW (2005) New developments in seismic risk assessment in Italy. Bulletin of Earthquake Engineering 3:101–128. https://doi.org/10.1007/s10518-005-0202-1

Dolce M, Kappos A, Masi A, et al (2006) Vulnerability assessment and earthquake damage scenarios of the building stock of Potenza (Southern Italy) using Italian and Greek methodologies. Eng Struct 28:357–371. https://doi.org/10.1016/j.engstruct.2005.08.009

Eads L, Miranda E, Krawinkler H, Lignos DG (2013) An efficient method for estimating the collapse risk of structures in seismic regions. Earthq Eng Struct Dyn 42:25–41. https://doi.org/10.1002/eqe.2191

Eads L, Miranda E, Lignos DG (2015) Average spectral acceleration as an intensity measure for collapse risk assessment. Earthq Eng Struct Dyn 44:2057–2073. https://doi.org/10.1002/eqe.2575

Eladly MM (2017) Numerical study on masonry-infilled steel frames under vertical and cyclic horizontal loads. J Constr Steel Res 138:308–323. https://doi.org/10.1016/j.jcsr.2017.07.016

Elnashai A, Di Sarno L (2015) Fundamentals of Earthquake Engineering: From Source to Fragility, 2nd edn. Wiley

EN 1991-1-4 (2004) Eurocode 1: Actions on structures - Part 1-4: General actions - Wind actions

Erkoseoglu G, Erberik MA, Citiloglu C (2014) A PARAMETRIC STUDY ON UNREINFORCED AND CONFINED MASONRY WALL BEHAVIOR . In: 2nd European Conference on Earthquake Engineering and Seismology (2ECEES). Istanbul

Farsangi EN, Noori M, Gardoni P, et al (2021) Reliability-Based Analysis and Design of Structures and Infrastructure. CRC Press, Boca Raton

FEMA (2012a) Hazus ®-MH 2.1 Technical Manual. Washington D.C.

FEMA (2024a) HAZUS 6.1 Earthquake Model Technical Manual . Washington, DC

FEMA (2024b) Hazus 6.1 Inventory Technical Manual. Washington, DC

FEMA (2012b) Next-Generation Methodology for Seismic Performance Assessment of Buildings, prepared by the Applied Technology Council for the Federal Emergency Management Agency, Report No. FEMA P-58. Washington, D.C.

Gaetani d'Aragona M, Polese M, Prota A (2020) Stick-IT: A simplified model for rapid estimation of IDR and PFA for existing low-rise symmetric infilled RC building typologies. Eng Struct 223:111182. https://doi.org/10.1016/j.engstruct.2020.111182

Gautam D, Chaulagain H (2016) Structural performance and associated lessons to be learned from world earthquakes in Nepal after 25 April 2015 (MW 7.8) Gorkha earthquake. Eng Fail Anal 68:222–243. https://doi.org/10.1016/j.engfailanal.2016.06.002

Gentile R, Galasso C (2021) Accounting for directivity-induced pulse-like ground motions in building portfolio loss assessment. Bulletin of Earthquake Engineering 19:6303–6328. https://doi.org/10.1007/s10518-020-00950-9

Gentile R, Galasso C (2022) Surrogate probabilistic seismic demand modelling of inelastic single-degree-of-freedom systems for efficient earthquake risk applications. Earthq Eng Struct Dyn 51:492–511. https://doi.org/10.1002/eqe.3576

Goda K, Atkinson GM (2011) Seismic performance of wood-frame houses in south-western British Columbia. Earthq Eng Struct Dyn 40:903–924. https://doi.org/10.1002/eqe.1068

Gondaliya KM, Amin J, bhaiya V, et al (2023) Seismic Vulnerability Assessment of Indian Code Compliant RC Frame Buildings. Journal of Vibration Engineering & Technologies 11:207–231. https://doi.org/10.1007/s42417-022-00573-1

Goulet CA, Kishida T, Ancheta TD, et al (2021) PEER NGA-East database. Earthquake Spectra 37:1331–1353. https://doi.org/10.1177/87552930211015695

Günay S, Mosalam KM (2013) PEER Performance-Based Earthquake Engineering Methodology, Revisited. Journal of Earthquake Engineering 17:829–858. https://doi.org/10.1080/13632469.2013.787377

Haach VG, Vasconcelos G, Lourenço PB (2010) Experimental Analysis of Reinforced Concrete Block Masonry Walls Subjected to In-Plane Cyclic Loading. Journal of Structural Engineering 136:452–462. https://doi.org/10.1061/(ASCE)ST.1943-541X.0000125

Heresi P, Miranda E (2021) Intensity Measures for Regional Seismic Risk Assessment of Low-Rise Wood-Frame Residential Construction. Journal of Structural Engineering 147:. https://doi.org/10.1061/(ASCE)ST.1943-541X.0002859

Jalayer F, Cornell CA (2009) Alternative non-linear demand estimation methods for probability-based seismic assessments. Earthq Eng Struct Dyn 38:951–972. https://doi.org/10.1002/eqe.876

Jalayer F, De Risi R, Manfredi G (2015) Bayesian Cloud Analysis: Efficient structural fragility assessment using linear regression. Bulletin of Earthquake Engineering 13:1183–1203. https://doi.org/10.1007/s10518-014-9692-z

Jalayer F, Ebrahimian H, Miano A, et al (2017) Analytical fragility assessment using unscaled ground motion records. Earthq Eng Struct Dyn 46:2639–2663. https://doi.org/10.1002/eqe.2922

Jamšek A, Dolšek M (2020) Seismic analysis of older and contemporary reinforced concrete frames with the improved fish-bone model. Eng Struct 212:110514. https://doi.org/10.1016/j.engstruct.2020.110514

Johnson K, Villani M, Bayliss K, et al (2023) Global Seismic Hazard Map

Jouneghani HG, Haghollahi A (2020) Assessing the seismic behavior of steel moment frames equipped by elliptical brace through incremental dynamic analysis (IDA). Earthquake Engineering and Engineering Vibration 19:435–449. https://doi.org/10.1007/s11803-020-0572-z

Karanikoloudis G, Lourenço PB (2018) Structural assessment and seismic vulnerability of earthen historic structures. Application of sophisticated numerical and simple analytical models. Eng Struct 160:488–509. https://doi.org/10.1016/j.engstruct.2017.12.023

Lallemant D, Kiremidjian A, Burton H (2015) Statistical procedures for developing earthquake damage fragility curves. Earthq Eng Struct Dyn 44:1373–1389. https://doi.org/10.1002/eqe.2522

Lang DH, Kumar A, Sulaymanov S, Meslem A (2018) Building typology classification and earthquake vulnerability scale of Central and South Asian building stock. Journal of Building Engineering 15:261–277. https://doi.org/10.1016/j.jobe.2017.11.022

Loss C, Piazza M, Zonta D (2013) A New Method to Assess the Seismic Vulnerability of Existing Wood Frame Buildings. Adv Mat Res 778:486–494. https://doi.org/10.4028/www.scientific.net/AMR.778.486

Lotfy I, Mohammadalizadeh T, Ahmadi F, Soroushian S (2022) Fragility Functions for Displacement-based Seismic Design of Reinforced Masonry Wall Structures. Journal of Earthquake Engineering 26:33–51. https://doi.org/10.1080/13632469.2019.1659881

Lu X, Han B, Hori M, et al (2014) A coarse-grained parallel approach for seismic damage simulations of urban areas based on refined models and GPU/CPU cooperative computing. Advances in Engineering Software 70:90–103. https://doi.org/10.1016/j.advengsoft.2014.01.010

Lu X, Tian Y, Wang G, Huang D (2018) A numerical coupling scheme for nonlinear time history analysis of buildings on a regional scale considering site-city interaction effects. Earthq Eng Struct Dyn 47:2708–2725. https://doi.org/10.1002/eqe.3108

Luzi L., Lanzano G., Felicetta C., et al (2020) Engineering Strong Motion Database (ESM) (Version 2.0)

Magenes G, Calvi GM (1992) Cyclic behaviour of brick masonry walls. In: 10th World Conference on Earthquake Engineering (10WCEE). A.A. Balkema, Rotterdam

Markulak D, Radić I, Sigmund V (2013) Cyclic testing of single bay steel frames with various types of masonry infill. Eng Struct 51:267–277. https://doi.org/10.1016/j.engstruct.2013.01.026

Martins L, Silva V (2021) Development of a fragility and vulnerability model for global seismic risk analyses. Bulletin of Earthquake Engineering 19:6719–6745. https://doi.org/10.1007/s10518-020-00885-1

Martins L, Silva V, Marques M, et al (2016) Development and assessment of damage-to-loss models for moment-frame reinforced concrete buildings. Earthq Eng Struct Dyn 45:797–817. https://doi.org/10.1002/eqe.2687

McCormick J, DesRoches R, Fugazza D, Auricchio F (2007) Seismic Assessment of Concentrically Braced Steel Frames with Shape Memory Alloy Braces. Journal of Structural Engineering 133:862–870. https://doi.org/10.1061/(ASCE)0733-9445(2007)133:6(862)

McKenna F (2011) OpenSees: A framework for earthquake engineering simulation. Comput Sci Eng 13:58–66. https://doi.org/10.1109/MCSE.2011.66

Murcia-Delso J, Shing PB (2012) Fragility Analysis of Reinforced Masonry Shear Walls. Earthquake Spectra 28:1523–1547. https://doi.org/10.1193/1.4000075

Nafeh AMB, Aljawhari K, Ettore A, et al (2026) OQ-VMTK: An Open-Source Toolkit for Earthquake Vulnerability Modelling Applications (UNDER REVIEW). Earthquake Spectra

Nafeh AMB, O'Reilly GJ (2024) Fragility functions for non-ductile infilled reinforced concrete buildings using next-generation intensity measures based on analytical models and empirical data from past earthquakes. Bulletin of Earthquake Engineering 22:4983–5021. https://doi.org/10.1007/s10518-024-01955-4

Nafeh AMB, O'Reilly GJ (2022) Unbiased simplified seismic fragility estimation of non-ductile infilled RC structures. Soil Dynamics and Earthquake Engineering 157:107253. https://doi.org/https://doi.org/10.1016/j.soildyn.2022.107253

National Research Institute for Earth Science and Disaster Resilience (2019) NIED K-NET, KiK-net

Nettis A, Gentile R, Raffaele D, et al (2021) Cloud Capacity Spectrum Method: Accounting for record-to-record variability in fragility analysis using nonlinear static procedures. Soil Dynamics and Earthquake Engineering 150:106829. https://doi.org/https://doi.org/10.1016/j.soildyn.2021.106829

Nucera F, Santini A, Tripodi E, Caliò I (2012) Seismic vulnerability assessment of confined masonry buildings by macro-element modeling: a case study. In: 15th World Conference on Earthquake Engineering (15WCEE). Lisbon

O'Reilly GJ (2021) Limitations of Sa(T1) as an intensity measure when assessing non-ductile infilled RC frame structures. Bulletin of Earthquake Engineering 19:2389–2417. https://doi.org/10.1007/s10518-021-01071-7

Parra PF, Arteta CA, Moehle JP (2019) Modeling criteria of older non-ductile concrete frame–wall buildings. Bulletin of Earthquake Engineering 17:6591–6620. https://doi.org/10.1007/s10518-019-00697-y

Perez Gavilan JJ, Flores LE, Alcocer SM (2015) An Experimental Study of Confined Masonry Walls with Varying Aspect Ratios. Earthquake Spectra 31:945–968. https://doi.org/10.1193/090712EQS284M

Porter K, Kennedy R, Bachman R (2007) Creating fragility functions for performance-based earthquake engineering. Earthquake Spectra 23:471–489. https://doi.org/10.1193/1.2720892

Radnić J, Baloević G, Matešan D, Smilović M (2013) On a numerical model for static and dynamic analysis of in-plane masonry infilled steel frames. Materwiss Werksttech 44:423–430. https://doi.org/10.1002/mawe.201300146

Raghunandan M, Liel AB, Luco N (2015) Aftershock collapse vulnerability assessment of reinforced concrete frame structures. Earthq Eng Struct Dyn 44:419–439. https://doi.org/10.1002/eqe.2478

Ramirez CM, Lignos DG, Miranda E, Kolios D (2012) Fragility functions for pre-Northridge welded steel moment-resisting beam-to-column connections. Eng Struct 45:574–584. https://doi.org/10.1016/j.engstruct.2012.07.007

Ricci P, Verderame GM, Manfredi G (2011) Analytical investigation of elastic period of infilled RC MRF buildings. Eng Struct 33:308–319. https://doi.org/10.1016/j.engstruct.2010.10.009

Romão X, Pereira N, Castro JM, et al (2021) European Building Vulnerability Data Repository

Sabelli R, Mahin S, Chang C (2003) Seismic demands on steel braced frame buildings with buckling-restrained braces. Eng Struct 25:655–666. https://doi.org/10.1016/S0141-0296(02)00175-X

Sen T (2009) Fundamentals of Seismic Loading on Structures. Wiley

Shedid MT, Drysdale RG, El-Dakhakhni WW (2008) Behavior of Fully Grouted Reinforced Concrete Masonry Shear Walls Failing in Flexure: Experimental Results. Journal of Structural Engineering 134:1754–1767. https://doi.org/10.1061/(ASCE)0733-9445(2008)134:11(1754)

Silva V (2019) Uncertainty and Correlation in Seismic Vulnerability Functions of Building Classes. Earthquake Spectra 35:1515–1539. https://doi.org/10.1193/013018EQS031M

Silva V, Amo-Oduro D, Calderon A, et al (2020) Development of a global seismic risk model. Earthquake Spectra 36:372–394. https://doi.org/10.1177/8755293019899953

Silva V, Brzev S, Scawthorn C, et al (2022) A Building Classification System for Multi-hazard Risk Assessment. International Journal of Disaster Risk Science 13:161–177. https://doi.org/10.1007/s13753-022-00400-x

Silveira D, Varum H, Costa A, et al (2018) Seismic behavior of two Portuguese adobe buildings: Part I - in-plane cyclic testing of a full-scale adobe wall. International Journal of Architectural Heritage 12:922–935. https://doi.org/10.1080/15583058.2017.1423131

So E (2016) Estimating Fatality Rates for Earthquake Loss Models. Springer

Soleimani R, Khosravi H, Hamidi H (2019) Substitute Frame and adapted Fish-Bone model: Two simplified frames representative of RC moment resisting frames. Eng Struct 185:68–89. https://doi.org/10.1016/j.engstruct.2019.01.127

Stafford PJ (2008) Conditional Prediction of Absolute Durations. Bulletin of the Seismological Society of America 98:1588–1594. https://doi.org/10.1785/0120070207

Suzuki A, Iervolino I (2021) Seismic Fragility of Code-conforming Italian Buildings Based on SDoF Approximation. Journal of Earthquake Engineering 25:2873–2907. https://doi.org/10.1080/13632469.2019.1657989

Suzuki A, Iervolino I (2020) Intensity measure conversion of fragility curves. Earthq Eng Struct Dyn 49:607–629. https://doi.org/10.1002/eqe.3256

Tarque N, Crowley H, Pinho R, Varum H (2012) Displacement-Based Fragility Curves for Seismic Assessment of Adobe Buildings in Cusco, Peru. Earthquake Spectra 28:759–794. https://doi.org/10.1193/1.4000001

Tarquini D, de Almeida JP, Beyer K (2019) Experimental investigation on the deformation capacity of lap splices under cyclic loading. Bulletin of Earthquake Engineering 17:6645–6670. https://doi.org/10.1007/s10518-019-00692-3

Tasnimi AA, Mohebkhah A (2011) Investigation on the behavior of brick-infilled steel frames with openings, experimental and analytical approaches. Eng Struct 33:968–980. https://doi.org/10.1016/j.engstruct.2010.12.018

Tischer H, Mitchell D, McClure G (2012) Ambient Vibration Measurements of Dynamic Properties of School Buildings in Montreal, Quebec. In: Structures Congress 2012. American Society of Civil Engineers, Reston, VA, pp 2279–2290

Ugalde D, Lopez-Garcia D (2020) Analysis of the seismic capacity of Chilean residential RC shear wall buildings. Journal of Building Engineering 31:101369. https://doi.org/10.1016/j.jobe.2020.101369

Ugalde D, Parra PF, Lopez-Garcia D (2019) Assessment of the seismic capacity of tall wall buildings using nonlinear finite element modeling. Bulletin of Earthquake Engineering 17:6565–6589. https://doi.org/10.1007/s10518-019-00644-x

Vamvatsikos D, Cornell CA (2002) Incremental dynamic analysis. Earthq Eng Struct Dyn 31:491–514. https://doi.org/10.1002/eqe.141

Vijayanarayanan AR, Goswami R, Murty CVR (2017) Estimation of Storey Stiffness in Multi-storey Buildings. In: Proceedings of the16th World Conference on Earthquake, 16WCEE, Santiago, Chile, January 9-13, 2017

Villar-Vega M, Silva V, Crowley H, et al (2017a) Development of a Fragility Model for the Residential Building Stock in South America. Earthquake Spectra 33:581–604. https://doi.org/10.1193/010716EQS005M

Villar-Vega M, Silva V, Crowley H, et al (2017b) Development of a fragility model for the residential building stock in South America. Earthquake Spectra. https://doi.org/10.1193/010716EQS005M

Voon KC, Ingham JM (2006) Experimental In-Plane Shear Strength Investigation of Reinforced Concrete Masonry Walls. Journal of Structural Engineering 132:400–408. https://doi.org/10.1061/(ASCE)0733-9445(2006)132:3(400)

Xiong C, Lu X, Guan H, Xu Z (2016) A nonlinear computational model for regional seismic simulation of tall buildings. Bulletin of Earthquake Engineering 14:1047–1069. https://doi.org/10.1007/s10518-016-9880-0

Yepes-Estrada C, Calderon A, Costa C, et al (2023) Global building exposure model for earthquake risk assessment. Earthquake Spectra 39:2212–2235. https://doi.org/10.1177/87552930231194048

Zareian F, Medina RA (2010) A practical method for proper modeling of structural damping in inelastic plane structural systems. Comput Struct 88:45–53. https://doi.org/10.1016/j.compstruc.2009.08.001